1   **A RAF-like kinase mediates a deeply conserved, ultra-rapid auxin response**

2

3   Andre Kuhn[1,*], Mark Roosjen[1,*], Sumanth Mutte[1], Shiv Mani Dubey[2], Polet Carrillo

4   Carrasco[1], Aline Monzer[3], Takayuki Kohchi[4], Ryuichi Nishihama[5], Matyáš Fendrych[2], Jiří

5   Friml[3], Joris Sprakel[1,6] and Dolf Weijers[1,#]

6

7   1, Laboratory of Biochemistry, Wageningen University, Stippeneng 4, Wageningen, the

8   Netherlands

9   2, Department of Experimental Plant Biology, Charles University, Prague

10   3, Institute of Science and Technology Austria, Klosterneuburg, Austria

11   4, Graduate School of Biostudies, Kyoto University, Kyoto, Japan

12   5, Department of Applied Biological Science, Faculty of Science and Technology Tokyo

13   University of Science, Noda, Chiba, Japan

14   6, Laboratory of Physical Chemistry and Soft Matter, Wageningen University, Wageningen,

15   the Netherlands

16

17   *, these authors contributed equally

18   #, corresponding author: dolf.weijers@wur.nl

19

20   Lead Contact: Further information and requests for resources and reagents should be directed

21   to and will be fulfilled by the lead contact, Dolf Weijers (dolf.weijers@wur.nl).

22

23

24

25

26

27

28

SUMMARY

The plant signaling molecule auxin triggers both fast and slow cellular responses across the plant kingdom, including both land plants and algae. A nuclear response pathway mediates auxin-dependent gene expression, and controls a range of growth and developmental processes in land plants. It is unknown what mechanisms underlie both the physiological responses occurring within seconds, and the responses in algae, that lack the nuclear auxin response pathway. We discovered an ultra-fast proteome-wide phosphorylation response to auxin across 5 land plant and algal species, converging on a core group of shared target proteins. We find conserved rapid physiological responses to auxin in the same species and identified a RAF-like protein kinase as a central mediator of auxin-triggered phosphorylation across species. Genetic analysis allowed to connect this kinase to both auxin-triggered protein phosphorylation and a rapid cellular response, thus identifying an ancient mechanism for fast auxin responses in the green lineage.

KEYWORDS

Auxin, protein phosphorylation, RAF kinase, plant evolution

INTRODUCTION

The plant signaling molecule is key to numerous growth and developmental processes in plants[1]. Iconic auxin-dependent processes are the tropic growth responses to light and gravity[2–5], differentiation of vascular strands and the control of fruit development[6–9]. The dominant naturally occurring auxin is indole 3-acetic acid (IAA), a chemically simple Tryptophan derivative that land plants can synthesize in a two-step pathway, but that is widely found across both prokaryotic and eukaryotic species[10]. While initial discoveries with auxin were made in flowering plants, both the occurrence of IAA and physiological and developmental responses to the molecule have been reported well beyond this group. All land plants studied[11], and a range of algae[12–14] show responses to externally applied auxin, which suggests a very deep origin of the capacity to respond to auxin. The cellular responses to auxin come in essentially two flavors: fast and slow. The fast responses include changes in membrane polarization[15–17], cytoplasmic streaming[18,19], Calcium and proton fluxes[20–24] and remodeling of the cytoskeleton[12,25] and trafficking[26]. Slower responses include cellular growth, division and differentiation[27–30].

Following an era of biochemical investigation that led to the identification of a set of auxin-binding proteins[31], genetic approaches have been incredibly successful in defining a comprehensive response system. Using the ability of auxin to inhibit root growth in the flowering plant *Arabidopsis thaliana* as a model, a set of components was identified that mediates auxin's activity in regulating gene expression – the nuclear auxin pathway (NAP)[32–36]. This system revolves around the auxin-triggered proteolysis of a family of transcriptional repressor proteins, thus liberating DNA-bound transcription factors and allowing gene regulation[37]. Through this pathway, auxin controls the expression of hundreds-thousands of genes, and mutations in its components interfere with most, if not all developmental auxin functions, culminating in embryo lethality in the most affected mutants[38–40].

As increasing numbers of plant genomes have become available, it became possible to reconstruct the occurrence and evolutionary history of the auxin response system. From such analysis, it appeared that the same auxin response system acts to control gene expression and development across land plants[11,41]. However, it is also clear that the closest sister group to land plants – the streptophyte algae – do not carry the NAP, in cases even lacking all its components[11]. Thus, a major unanswered question is how algae can respond to auxin in the absence of the known auxin response system. In addition, the fastest gene expression

84   responses to auxin have been recorded in 5-10 minutes[42,43], but several of the fast

85   responses[18,19,23,44,45] occur within seconds, or at least well within the time needed for gene

86   expression and protein synthesis. Thus, it is likely that the currently known auxin response

87   system represents the "slow" branch, and that a separate, currently unknown system must

88   exist to mediate fast responses. The existence of fast auxin responses in land plants and their

89   algal sisters would predict such a system to be shared between these clades.

90   Building on the rich literature in animal signaling, we explored the hypothesis that

91   regulated protein phosphorylation may represent a mechanism mediating fast auxin responses.

92   In the accompanying article (Roosjen, Kuhn et al., accompanying manuscript) we

93   demonstrate that auxin can trigger changes in protein phosphorylation well within 30 seconds,

94   and that more than 2000 proteins are targeted by auxin-triggered phosphorylation within 10

95   minutes in Arabidopsis roots. Auxin-triggered phosphorylation targets numerous pathways,

96   including those leading to changes in membrane polarity. Here, we asked if this novel auxin

97   response may represent the elusive, deeply conserved mechanism underlying rapid cellular

98   responses. We indeed find that auxin triggers rapid changes in protein phosphorylation in 5

99   different land plant and algal species, including a core set of conserved targets. We show that

100   auxin has deeply conserved activity in accelerating cytoplasmic streaming and membrane

101   polarity. Lastly, we identify a key RAF-like kinase that mediates auxin-triggered protein

102   phosphorylation and control of fast cellular responses across species. This work thus identifies

103   an ancient system for rapid responses to the auxin signaling molecule.

104

105 **RESULTS**

106

107 **Identification of a deeply conserved, rapid, phosphorylation-based auxin response**

108

109 To examine whether the rapid phosphorylation-based auxin response that we have identified

110 in *Arabidopsis thaliana* roots (Henceforth: Arabidopsis; Roosjen, Kuhn et al, accompanying

111 manuscript) is conserved beyond this species, we selected a set of phylogenetically distant

112 species ranging from green algae to bryophytes for phosphoproteomic analysis. These

113 included the streptophyte algae *Klebsormidium nitens* (Klebsormidium) and *Penium*

114 *margaritaceum* (Penium) and the bryophytes *Marchantia polymorpha* (Marchantia) and

115 *Physcomitrium patens* (Physcomitrium) in addition to the angiosperm Arabidopsis. This

116 selection encompasses both early-diverging streptophyte algae (Klebsormidium) and a close

117 sister to land plants (Penium; Zygnematophyceae), and covers two clades within the

118 bryophytes: liverworts (Marchantia) and mosses (Physcomitrium). Notably, while sporophytic

119 (root) tissue was sampled for Arabidopsis, gametophyte tissue was sampled for all other

120 species. Thus, the suite of species not only spans phylogeny, but also haploid and diploid

121 generations. All species were treated with the same concentration (100 nM) of the naturally

122 occurring auxin Indole 3-Acetic Acid (IAA, auxin), followed by phosphopeptide enrichment

123 after two minutes using the same experimental, mass spectrometry and analysis workflow that

124 we describe in Roosjen, Kuhn et al. (accompanying manuscript). Strikingly, we find that two

125 minutes of auxin treatment leads to large shifts in the phospho-proteome in all species tested

126 (Figure 1A). The number of differential phosphosites was comparable across species

127 (FDR$\geq$1.301: n=1048 in Arabidopsis; n=670 in Physcomitrium; n=741 in Marchantia; n=719

128 in Penium; n=1231 in Klebsormidium). In all species except Klebsormidium,

129 hyperphosphorylation upon auxin treatment represented the majority of differential

130 phosphosites (64% in Arabidopsis, 76% in Physcomitrium, 73% in Marchantia and 60% in

131 Penium), while hyper- and hypophosphorylation were more equal in Klebsormidium (47%

132 hyperphosphorylation) (Figure 1A). Thus, rapid, global changes in phospho-proteomes are

133 triggered by auxin at comparable scale in all species tested.

134 We next asked if the cellular functions and proteins that are targeted by auxin-

135 triggered phosphorylation changes are conserved among the species tested. Estimated

136 divergence times of the species used here from common ancestors is around 850 Mya for

137 algae and land plants, and 500 Mya among the land plants[46]. Given these enormous

138 evolutionary distances, there is substantial sequence divergence within protein families, and

139   large differences in gene family numbers[47]. This makes establishing direct orthology

140   relationships very challenging. Therefore, before comparison of differential phosphoproteins

141   at protein/family level, we first constructed a set of orthogroups that represent the set of genes

142   that originated from a single gene in the last common ancestor of all the species under

143   consideration. We then consider members of the same orthogroup to represent a conserved

144   ancestral function. Among the species tested, Penium has a remarkably large number of

145   orthogroups with multiple members within Penium (Figure 1B), which is a reflection of the

146   high degree of fragmentation of the genome assembly[48].

147   Comparing the phosphosites in all species, we found an overlap of 11 orthogroups

148   across all organisms (Figure 1C). Given the previous consideration, we also consider

149   orthogroups not represented in Penium to be relevant. When excluding Penium from the

150   analysis we found 29 orthogroups to be shared (Figure 1C). Gene Ontology (GO) analysis on

151   the conserved orthogroups showed that a broad range of cellular functions is subject to auxin

152   regulation (Figure 1D). These include processes at the plasma membrane or endomembranes,

153   such as transmembrane transport and clathrin coat disassembly, but also nuclear organization

154   and posttranslational regulation of gene expression. Furthermore, GO analysis identified

155   responses to external stimuli and hormones, including response to blue light, abscisic acid

156   transport and polar auxin transport. As expected from a phospho-proteomic analysis, protein

157   phosphorylation was another highly enriched GO-term. In line with that, we find RAF-like

158   kinases and the blue-light receptor PHOT1 as a conserved target of auxin-triggered

159   phosphorylation (Figure 1E).

160   Limiting GO analysis to only the 29 conserved orthogroups is very stringent, as it is

161   strongly constrained by sequence similarity, which may be limited across such long

162   evolutionary timescales. We therefore also performed GO analysis on the full set of

163   differentially phosphorylated phosphosites (FDR≤0,05) in each species separately, and

164   compared the enriched GO-terms. This comparison found 7 GO-terms enriched in all species

165   tested (Figure 1F), suggesting that these represent core target processes of rapid auxin

166   response. Beyond the previously identified GO terms (Figure 1D), "transmembrane transport"

167   and "proton transmembrane transport" were highly enriched (Figure 1G). Further analysis

168   showed that in all species tested, H^+-ATPase proton pumps were differentially phospho-

169   regulated upon auxin treatment (Figure 1H). Clearly, there were also many GO-terms that

170   were uniquely enriched in one or a few species (Figure 1F), suggesting that rapid auxin-

171   triggered phosphorylation not only has a conserved component, but also a species/lineage-

172 specific component. In conclusion, auxin triggers a conserved set of rapid phosphorylation

173 changes across land plants and algae, converging on shared cellular processes.

174

175 **Auxin triggers fast cellular and physiological responses across the plant lineage**

176

177 The identification of a deeply conserved auxin response that targets a common set of proteins

178 and functions, suggests that there are cellular processes that auxin can regulate across the

179 green kingdom. Among the fast auxin responses that have previously been recorded (see

180 introduction), two stand out as being potential candidates for being shared outside of land

181 plants. We explored whether auxin can trigger changes in membrane polarity and cytoplasmic

182 streaming across species.

183 Membrane potential reflects the difference between cytoplasmic and apoplastic

184 electrical potentials (Figure 2A). Auxin has a profound effect on membrane potential by

185 triggering instantaneous depolarization of plasma membranes. This depolarization is then

186 followed by a hyperpolarization of the membrane[17,24]. Both membrane depolarization and

187 hyperpolarization depend on auxin's ability to regulate ion fluxes across the plasma

188 membrane, prominently involving H^+-ATPase proton pumps[17,23,49,50]. To test whether this

189 response is conserved in the plant lineage, we monitored membrane potential after 5 min of

190 treatment with 100 nM auxin in Arabidopsis roots, Marchantia gemmae and Klebsormidium

191 filaments using the membrane potential fluorescent probe $DISBAC_2(3)$ [17,51]. Increase in

192 $DISBAC_2(3)$ fluorescence reports membrane depolarization[17,51]. We observed a significant

193 increase of fluorescence ratio upon auxin-treatment in all three species (Figure 2A).

194 Moreover, the increase was quantitatively very similar between species. This indicates that

195 rapid auxin-triggered plasma membrane depolarization is a deeply conserved rapid auxin

196 response.

197 Cytoplasmic streaming describes the movement of organelles along the actin

198 cytoskeleton and is thought to have essential function in transport of nutrient and proteins

199 within the cell [52]. In plants, cytoplasmic streaming is thought to be primarily driven by plant-

200 specific Myosin XI cytoskeletal motor proteins[52]. We found that in Arabidopsis, Myosin XI-K

201 and the MadB Myosin-binding proteins are targets of rapid auxin-dependent

202 physophorylation[53], and that auxin promotes cytoplasmic streaming in root epidermal cells[18].

203 We examined the physiological effect of 100 nM auxin on cytoplasmic streaming by

204 monitoring the movement of fluorescently labeled mitochondria in epidermis cells within the

205 root elongation zone in Arabidopsis and in Marchantia rhizoid cells (Figure 2B). After
206 particle tracking, we determined the active diffusion rate (K) and diffusive exponent (α) by
207 fitting mean-square displacements, ensemble-averaged per cell, to the anomalous diffusion
208 model, in both auxin treated and untreated samples. We detected consistent streaming within
209 both species, but found absolute rates to differ among species (Figure 2B). Pretreatment of
210 Arabidopsis roots with the actin depolymerizing drug Latrunculin B reduced cytoplasmic
211 streaming in both species (Supplementary Figure 1B), thus implicating the actin cytoskeleton.
212 Importantly, auxin treatment increased the diffusion rate in all species tested (Figure 2B).
213 Hence, like membrane depolarization, acceleration of cytoplasmic streaming is a deeply
214 conserved cellular response to auxin.
215
216 **Identification of RAF-like kinases as conserved components in auxin response**
217
218 The finding that there are conserved phosphorylation responses to auxin in algae and land
219 plants, along with conserved cellular responses, suggests the existence of a shared mechanism
220 for auxin perception and signal transduction. Given the prominent phosphorylation changes
221 across species and the temporal dynamics of the response in Arabidopsis (Roosjen, Kuhn et
222 al, accompanying manuscript), we anticipate a key role for auxin-activated protein kinases. To
223 identify such kinases, we first analyzed phosphorylation motifs enriched among the conserved
224 phospho-targets. We found that hyperphosporylation was associated with the presence of a
225 proline-directed SP motif (Figure 3A). These are typically targeted by MAP kinases[54,55].
226 Indeed, when inferring kinase-target networks in Arabidopsis from temporal phosphorylation
227 profiles and activation loop phosphorylation predictions, we identified an auxin-activated
228 RAF-like Kinase as a potential hub, central to the phosphorylation network (Roosjen, Kuhn et
229 al., accompanying manuscript). Strikingly, orthologues of this same Rapidly Accelerated
230 Fibrosarcoma (RAF)-like kinase were hyperphosphorylated upon auxin treatment in all other
231 species tested (Figure 1E and 3B), except in Penium, where genome assembly fragmentation
232 likely precluded its identification. In addition to the RAF-like kinase, we also identified
233 PHOT1 as a conserved target of auxin-triggered hyperphosphorylation (Figure 1E). However,
234 given the multiple lines of evidence suggesting a role for the RAF-like Kinases in auxin-
235 triggered phosphorylation, we here focus on this protein.
236   RAF-like kinases are serine/threonine kinases that belong to the mitogen activated
237 protein kinase kinase kinases (MAPKKKs) family. They are classified into four B clades and
238 seven C clades according to their homology with the widespread eukaryotic RAF protein

239 kinases[56]. Arabidopsis B2, B3 and B4 clade RAF-like kinases have been implicated in various

240 physiological responses, including responses to hypoxia, osmotic stress and drought[57,58]. The

241 Marchantia B4 RAF-like kinase (PRAF) was implicated in the regulation of carbon fixation[59].

242 While we found RAF-like kinases of the B2, B3 and B4 clade to be hyperphosphorylated after

243 auxin treatment in Arabidopsis, it seems that only hyperphosphorylation of RAF-like kinases

244 of the B3 and B4 clade upon auxin treatment is conserved (Figure 1E). The B4 clade is

245 represented by 7 paralogs in Arabidopsis, 2 in Physcomitrium and single copies in

246 Klebsormidium and Marchantia[60] (Figure 3C). Most of these are hyperphosphorylated in

247 response to auxin treatment (Figure 3B), firmly connecting this family to auxin response. We

248 refer to these proteins as MAP AUXIN RESPONSIVE KINASE/RAFs (MARK/RAFs).

249   Given that no role for these proteins in auxin response has been reported, we initially

250 explored requirements for MARK/RAF kinases in auxin-associated growth and development,

251 as well as in response to externally applied auxin. To this end, we analyzed previously

252 established mutants: two septuple mutants of the entire Arabidopsis B4 clade either conferring

253 a null (*mark/raf*[null]; also referred to as OK[130]-*null* [58]) or a weak allele combination

254 (*mark/raf*[weak]; also referred to as OK[130]-*weak*[58]), and a null mutant in the single Marchantia

255 ortholog (Mp*mark/praf*[KO], also referred to as Mp*praf*[KO 59]). We found that in both species,

256 loss of MARK activity caused growth and developmental phenotypes (Figure 3D). While in

257 Arabidopsis we found a range of defects in root growth, plant height and rosette area and

258 germination (Figure 3D; Supplementary Figure 2), in Marchantia, these manifested as smaller

259 thallus size and reduced gemmae cup number confirming previously published results[59]

260 (Figure 3D; Supplementary Figure 2). Essentially all these processes are known to involve

261 auxin action[30,61,62]. We therefore tested sensitivity of the Arabidopsis and Marchantia

262 *mark/praf* mutants to auxin. In Arabidopsis, *mark* mutant roots were slightly less sensitive to

263 growth inhibition by auxin (Figure 3E). Likewise, Marchantia *mark/praf* mutant thallus,

264 although already under control conditions reduced in size, was also less sensitive to auxin-

265 induced growth inhibition (Figure 3F). Thus, in both species, MARK/RAF kinases act in

266 growth and development, and play a role in auxin response.

267

268 **MARK kinases mediate fast auxin phospho-response**

269

270 Auxin-associated growth and development, as well as Arabidopsis root and Marchantia

271 thallus growth responses to externally applied auxin is typically associated with changes in

272 auxin-dependent gene expression through the NAP[37,41]. given the auxin-related phenotypes in

273   *mark* mutants, we asked if these are affected in transcriptional responses. We therefore

274   performed RNA-Seq in Arabidopsis (roots) and Marchantia (thallus) wildtype and *mark/raf*

275   mutants that were either treated with 1μM IAA or control medium for one hour. This

276   concentration of IAA should allow to detect even subtle changes in transcription in mutants.

277   In both species, transcriptomes under untreated conditions look very distinct between mutant

278   and wildtype (Figure 4A,B), suggesting massive effects of loss of MARK/RAF function on

279   the "baseline" transcriptome in the absence of externally applied auxin. However, comparing

280   auxin-treated and untreated samples in both species showed substantial auxin-induced

281   changes in transcriptomes in both wildtypes and in *mark/raf* mutants (Figure 4A,B).

282   Qualitatively, mutants in both species still showed a typical gene expression response to

283   auxin. Indeed, detailed analysis of individual auxin-regulated genes (Figure 4A,B) showed

284   that mutants did not have an obvious defect in auxin-induced transcription. This suggests that

285   MARK/RAF proteins do not have a major role in transcriptional auxin responses.

286   Given the rapid activation of MARK/RAF kinases by auxin (Figure 3B), it is

287   conceivable that these kinases act in auxin response through their role in mediating rapid

288   phosphorylation responses. We tested this hypothesis by subjecting *mark/raf* mutants in both

289   Arabidopsis and Marchantia to phosphoproteomic profiling after two minutes of treatment

290   with 100 nM IAA or control media. In both species, we found that the number of significant

291   differential hyperphosphorylated phosphosites after auxin treatment was reduced (666 in

292   Arabidopsis WT; 445 in At*mark/raf* mutant; 538 in Marchantia WT; 285 in Mp*mark/praf*;

293   Figure 4C). When comparing the number of phosphosites in wild-types and mutants, we

294   found that 73% of the differential phosphosites in wild-type was lost in the Arabidopsis

295   *mark/raf* mutant, while 51% was lost in the Marchantia *mark/praf* mutant (Figure 4C). We

296   compared phosphoproteomes in non-treated mutants with wild-type controls in both species to

297   identify functions that are deregulated in *mark* mutants. In Arabidopsis *mark/raf*, 392

298   orthogroups were different between mutant and wildtype, while in Marchantia *mark/praf,* 785

299   orthogroups were differentially phosphorylated (Figure 4D). Many orthogroups that were not

300   significantly affected by auxin in wild-type became differentially phosphorylated upon auxin

301   treatment in the mutants (Figure 4E). This suggests that the mutants in both species not only

302   lack a substantial part of auxin-triggered phosphorylation, but also have a response system

303   that is differently wired in non-treated conditions. This is consistent with the large

304   transcriptional changes, and with the strong phenotypes in the mutants. When comparing

305   targets of MARK-dependent, auxin-triggered phosphorylation changes in the two species, we

306   found a small overlap (24 orthogroups; Figure 4E). Given the evolutionary distance between

307 Marchantia and Arabidopsis, this is remarkable since it suggests that there is indeed a set of
308 evolutionary conserved fast auxin response under control of a conserved mechanism. These
309 shared, MARK/auxin-dependent targets included proteins associated with a diverse set of
310 cellular processes (Figure 4F; Supplementary Figure 3A). This includes ion transport,
311 membrane dynamics, and auxin export (e.g. PIN's, ABCB's, D6PK), but also featured nuclear
312 processes such as splicing and cytoplasmic processes such as cell plate formation and
313 cytoskeleton organization (e.g. SPIKE1, TOR1, NEK5). Lastly, this analysis also identified
314 previously reported phospho-targets of B4-type RAF kinases (e.g. VCS, VCR, SE).

315   To explore to what extent the auxin-triggered phosphorylation network is affected in
316 *mark* mutants, we compared the phosphorylation state of all kinases that were significantly
317 hypo- or hyperphosphorylated upon auxin treatment in wild-type of both species with their
318 phosphorylation state in *mark* mutants. Notably, in *mark* mutants, most of the auxin-triggered
319 kinase phosphorylation was lost (Figure 4G,H). This suggests that MARK/RAFs directly or
320 indirectly regulates the auxin-triggered phosphorylation of these kinases.

321

322 Specificity and mechanism of MARK activation

323

324 Proteins in the Arabidopsis MARK/RAF family have been identified as being
325 hyperphosphorylated upon osmotic treatment[58] and to mediate response to hypoxia[57], while
326 Marchantia MARK/PRAF has a role in the response to altered photosynthesis[59]. This suggests
327 that the same kinase is part of multiple response pathways and urges the questions of how
328 specific the auxin-triggered phosphorylation changes are, and how MARK/RAF is activated
329 in the context of auxin response. We initially compared the 2-minute auxin-triggered
330 phosphorylation changes with the set of 973 phosphosites that are osmotic stress-responsive
331 in Arabidopsis[58]. The overlap was very limited (37 phosphosites; Supplementary Figure 3B),
332 and 13 of these overlapping phosphosites depend on MARK/RAF (Supplementary Figure
333 3B). We therefore conclude that the phosphoresponse that we identified here is specific and
334 independent from osmotic stress responses.

335   We next explored mechanisms of MARK/RAF activation. In time-course
336 phosphoproteome data (derived from Roosjen, Kuhn et al., accompanying manuscript), we
337 found that multiple sites on all AtMARK/RAF proteins are modulated upon auxin treatment
338 (Figure 5A), suggesting profound and rapid regulation. As part of our characterization of the
339 auxin-triggered fast phosphoproteome in Arabidopsis, we found that the ABP1 auxin binding
340 protein and the TMK1 receptor-like kinase as well as the intracellular AFB1 receptor

341 contribute to effects of auxin on the phosphoproteome (Friml et al., 2022; Roosjen, Kuhn et

342 al., accompanying manuscript). We found that phosphoproteome changes in *abp1* and *tmk1*

343 mutants are highly correlated (Roosjen, Kuhn et al., accompanying manuscript), while effects

344 on the same phosphosites in *afb1* mutants often are anticorrelated (Roosjen, Kuhn et al.,

345 accompanying manuscript). We compared the Arabidopsis *mark* mutant phosphoproteomes

346 with those of wild type, *afb1, abp1* and *tmk1* mutants and found that phosphosites in *mark/raf*

347 phosphoproteomes overlap less with those of *afb1*-3 and the auxin-treated wildtype

348 phosphoproteome than with those of *tmk1* and *abp1* (Figure 5B,D). This is true for both *mark*

349 phosphoproteomes in control and auxin-treated conditions. suggesting that the *mark*

350 phosphoproteome under mock conditions is already strongly distorted. Given that

351 MARK/RAFs do not have a clear ligand-binding domain, we were interested to see if

352 MARK/RAFs phoshorylation depends on ABP1/TMK1 and/or AFB1. Therefore, we arrayed

353 all phosphosites in AtMARK's and compared their phosphorylation state in the mutant

354 backgrounds (Figure 5C). In this analysis it is clear that MARK/RAF phosphorylation is

355 strongly disturbed in each mutant, and that the *afb1* pattern more closely resembles that of

356 wild-type, whereas *abp1* and *tmk1* more severely disturb MARK/RAF phosphorylation

357 (Figure 5C). Interestingly, consistent with global patterns of the entire phosphoproteome

358 (Roosjen, Kuhn et al, accompanying manuscript), for some MARK/RAF sites,

359 phosphorylation is antagonistically distorted between *afb1* mutants and *abp1* and *tmk1*

360 mutants.

361

362 **MARK links rapid phospho-response to fast auxin responses**

363

364 MARK/RAF proteins are a unique family of kinases that carry an N- terminal Phox-Bem1

365 domain (PB1)[63] in addition to their C-terminal kinase domain (Figure 3B). PB1 domains can

366 either mediate heterotypic or homotypic protein interaction with other PB1 domains, which

367 can assemble into dimers or oligomers[64,65]. Apart from a single Arabidopsis paralog

368 (HCR1)[57], MARK/RAF protein localization has not been studied. We therefore generated

369 translational fusions of Arabidopsis and Marchantia MARK/RAF proteins to fluorescent

370 proteins and determined their localization. In both species, MARK/RAF proteins localized to

371 punctate structures (Figure 6A, B) resembling the "punctae" observed for other PB1-

372 containing proteins[66–68]. In both Arabidopsis roots (Figure 6A) and Marchantia gemmae

373 (Figure 6B), these structures were associated both with the plasma membrane and in the

374 cytoplasm. Thus, MARK/RAF protein locates to sites where fast auxin responses occur.

375   Given the profound role of MARK/RAF in mediating fast auxin-triggered

376   phosphorylation changes, we explored whether MARK/RAF might mediate the rapid effect of

377   auxin on membrane potential and cytoplasmic streaming. Responses to auxin treatment in

378   membrane depolarization were normal in *mark* mutants in both Arabidopsis and Marchantia

379   (Figure 6C, Supplementary Figure 4). However, we did find that Arabidopsis *mark/raf*

380   mutants showed an altered apoplastic root surface pH profile (Supplementary Figure 5),

381   perhaps caused by altered developmental zonation. Nonetheless, MARK/RAF does not appear

382   to mediate auxin-triggered membrane depolarization (Figure 6C, Supplementary Figure 4)

383   and the root surface alkalization response (Supplementary Figure 5).

384   In contrast, already in untreated Arabidopsis *mark/raf* mutant root epidermal cells,

385   cytoplasmic streaming is significantly reduced (Figure 6D; compare with Figure 2B).

386   Interestingly, *mark/raf* mutants are essentially insensitive to the promoting effect of auxin in

387   cytoplasmic streaming (Figure 6D). In Marchantia rhizoid cells, *mark/praf* mutants showed

388   wild-type cytoplasmic streaming in untreated conditions, but like in Arabidopsis, mutant cells

389   were insensitive to the promoting effect of auxin (Figure 6D; compare with Figure 2B). This

390   suggests that MARK proteins have a conserved role in mediating auxin-promoted cytoplasmic

391   streaming in Arabidopsis and Marchantia. Collectively, we conclude that MARK proteins link

392   rapid phosphorylation changes to a fast cellular response to auxin.

393

394

395

DISCUSSION

Over the past decades, there have been impressive advances in understanding how auxin is synthesized, transported and degraded, and how it controls plant growth and development by regulating gene expression[37]. There are however several major open questions. Firstly: there is a number of auxin responses that are too rapid to be mediated by gene regulation, for which there is no mechanism yet. Secondly, no known mechanism can account for responses to auxin in algae, that lack the well-known transcriptional auxin response system[11]. In the accompanying article (Roosjen, Kuhn et al., accompanying manuscript) we identify a fast, unknown and unsuspected branch of auxin activity based on rapid protein phosphorylation, in Arabidopsis roots. Here, we demonstrate that this pathway is conserved across the green lineage, extending beyond land plants into the streptophyte algae. We show that some fast cellular responses to auxin are also conserved across land plants and algae and identify a key protein kinase mediating both auxin-triggered phosphorylation and a rapid cellular response. This identifies rapid phosphorylation-dependent signaling as a mechanism that can account for both fast and deeply conserved auxin responses.

Although we compared phosphoproteomes in different tissue types, and in both sporophytic (for Arabidopsis) and gametophytic tissue (for all other species), we detected a core set of functions and orthologous protein groups that are shared between all. The most parsimonious explanation is that this core set represents a truly ancient auxin "regulome" that has been retained in all these species to serve core functions. This is not trivial, given the estimated divergence times of between 850-500 Mya. In addition to the core set, there are numerous lineage/clade/group/organism-specific targets. This suggests profound diversification and neo-functionalization of auxin-triggered phosphorylation pathways. We have compiled all phosphoproteomics data generated in this study in the AuxPhos webtool (https://weijerslab.shinyapps.io/AuxPhos; Roosjen, Kuhn et al., accompanying manuscript), to allow facile access.

Though mining both comparative phosphoproteomics, kinase-substrate inference from temporal series and motif analysis, we identified a family of B4 RAF-like kinases (MARK/RAFs). Exploring mutants in orthologous proteins in Arabidopsis and Marchantia, we could establish that MARK/RAF kinases are central to auxin-triggered phosphorylation, and to development and physiological and cellular auxin response. Curiously, transcriptional auxin responses are not impaired, which suggests that the rapid, phosphorylation-based

428   pathway is mechanistically uncoupled from the nuclear auxin pathway. The mutants, even in

429   the absence of auxin treatment, have dramatic phenotypes. It should however be kept in mind

430   that members of the MARK/RAF family have been implicated in responses to other triggers

431   (e.g. light, osmotic stress)[57–59]. Disruption of these responses likely also contribute to the

432   strong phenotypes, and dedicated strategies will be required to deconvolute these roles.

433   Notably, regulation of most kinases that are differentially phosphorylated upon auxin

434   treatment in wild-type Marchantia and Arabidopsis, is lost in *mark* mutants, suggesting that

435   MARK/RAF may sit at the apex of a multi-tier phosphorylation network. Interestingly, RAF

436   kinases, MARK/RAF orthologs in mammals, play an important role as master regulator of

437   signaling cascades, for example in EGF signaling[65]. MARK phosphorylation upon auxin

438   treatment occurs within 30 seconds in Arabidopsis (the earliest sampled timepoint; Roosjen,

439   Kuhn et al., accompanying manuscript). Mammalian RAF kinases can be activated by

440   phosphorylation within seconds to minutes after signal recognition[69,70]. Therefore, the kinetics

441   of MARK/RAF activation is consistent with the phospho-activation of their orthologs in

442   animal cells.

443   Mammalian RAF Kinases polymerize through their PB1 domain and localize in

444   punctate structures in the cytoplasm to form so-called signalosomes[65,68]. Signalosomes are

445   large supramolecular protein complexes that help increase avidity between signaling

446   components. The formation of such signaling hubs and their association with receptors is

447   crucial for signal transduction in some pathways[64]. Curiously, both Arabidopsis and

448   Marchantia MARK/RAF proteins localize to punctate structures in the cytoplasm and at the

449   plasma membrane. It will be interesting to see if these punctae are functional signalosomes,

450   whether they form through PB1 domain oligomerization, and what other proteins they bring

451   together.

452   Inspired by the finding that algae and land plants share a common set of auxin

453   phosphotargets, we explored if there are also shared cellular and physiological responses.

454   Indeed, cytoplasmic streaming is deeply conserved responses across land plants while

455   membrane depolarization is deeply conserved across land plants and algae. Both are

456   widespread cellular phenomena that are connected to for example cellular growth, nutrient

457   distribution and acquisition[50,71,72]. It is not clear what function the auxin-regulation of these

458   processes serves, but analysis of these responses in *mark/raf* mutants did help to show

459   bifurcation of rapid auxin response mechanisms. While auxin-dependent acceleration of

460   cytoplasmic streaming depended on MARK/RAF, membrane depolarization did not.

461   Interestingly, *mark/raf* mutants already had lower streaming velocity in the absence of auxin
462   treatment, suggesting the same pathway operates during normal development, likely
463   mediating the response to endogenous auxin.

464   The differential roles of MARK/RAF in the regulation of cytoplasmic streaming and
465   membrane polarity are conserved between Arabidopsis and Marchantia, suggesting a deep
466   evolutionary split between these two functions. In Arabidopsis, auxin-triggered membrane
467   depolarization was previously attributed to the cytoplasmic AFB1 auxin receptor[17], but its
468   mechanism of action is not yet clear. Interestingly, AFB1 is a late innovation specific to
469   angiosperms, and auxin-triggered membrane depolarization is found in the alga
470   Klebsormidium that does not carry any TIR1/AFB ortholog[11]. This raises the question how
471   the auxin signal translates to membrane depolarization outside of the angiosperms. Apart of
472   the MARK/RAF-family, we identified B3-clade RAF-like kinases and PHOT1 kinases as
473   potential conserved hubs in the auxin phosphorylation. It will be interesting to see if these
474   kinases play a role in regulating membrane depolarization. Interestingly, PHOT1 was
475   previously shown to mediate a rapid blue light-triggered membrane depolarization in
476   Arabidopsis[73], making it a strong candidate.

477   A key question is how the auxin signal is perceived and transmitted onto MARK/RAF
478   proteins, given that MARK/RAFs do not have a clear ligand-binding domain. The auxin
479   response components ABP1, TMK1 and AFB1 all contribute to auxin-triggered
480   phosphorylation changes in Arabidopsis (Roosjen, Kuhn et al., accompanying manuscript).
481   MARK/RAF phosphorylation was disturbed in all three mutants, but is clear from global
482   phosphoproteomes that the response is not linear, and likely relatively complex. MARK/RAF
483   kinases now offer a strong starting point to mechanistically dissect the response pathway,
484   including its receptor. It is encouraging that ABP1 is deeply conserved among land plants and
485   algae (Supplementary Figure 6). While no clear ortholog is present in Marchantia[74], ABP1 is
486   member of the large Cupin family, and other members of this family in Arabidopsis also
487   appear to function as auxin receptors [75 co-submitted manuscript]. This raises the interesting possibility
488   that the broader Cupin family, represented in all domains of life[76], may act as auxin receptors
489   for fast responses, including those mediated by MARK/RAF.

490   One striking aspect of the phosphorylation response we have discovered, is that it
491   clearly predates the origin of the nuclear auxin response pathway[11]. Thus, well before the
492   innovations appeared that led to auxin-dependent gene regulation, algal cells possessed a

493   system to rapidly respond to auxin. The nuclear auxin response did not evolve to replace this

494   system, as the rapid response system has been retained in land plants. Thus, the rapid system

495   likely regulates responses that the nuclear system cannot, and vice versa. This could in part

496   reflect the fundamental difference in auxin controlling cellular physiology and cell identity

497   and fate, which happen at very different timescales. The description of this response and its

498   deep origin, and the identification of the first component, now opens avenues to genetically

499   and biochemically characterize these pathways in the future. This will likely deepen our

500   understanding on the origins of auxin signaling and help reveal the ancestral role of auxin

501   within the green lineage.

502

503

AUTHOR CONTRIBUTIONS,

Conceptualization: A.K., M.R., D.W.; Methodology: A.K., M.R., P.C.C., S.M., S.M.D., J.S.; Formal analysis: M.R., A.K., P.C.C., S.M., S.M.D., A.M., M.F., J.S..; Investigation: A.K., M.R., P.C.C., S.M., S.M.D., A.M.; Resources: R.N., T.K.; Writing – Original Draft: A.K., D.W.; Writing – Review & Editing: all authors; Visualization: A.K., M.R., P.C.C., S.M., S.M.D.; Supervision: M.F., J.F., J.S., D.W.; Funding Acquisition: A.K., M.F., J.F., J.S., D.W..

DECLARATION OF INTERESTS

None of the authors have competing interest to declare.

MATERIALS AND METHODS

534

535

Plant material and culture conditions

536

All plants were cultured under 90-100 μmol photons m^{-2} s^{-1} white light with a 16 h light / 8

537

dark cycle at 22 °C and 75% humidity. *Arabidopsis thaliana* wild type Columbia-0 (Col-0)

538

and all Arabidopsis mutants and transgenics were cultured on half strength Murashige and

539

Skoog (MS) basal medium [77] at pH 5.7 supplemented with 0.8 % agar. All Arabidopsis

540

mutants use were previously published: *tmk1-1* (SALK_016360) [78], *abp1-td1* [79], *afb1-3* [80],

541

mark/raf^{null} (published as OK^{130null}) [58] and *mark/raf^{weak}* (published as OK^{130weak}) [58].

542

Marchantia polymorpha wild type strain Takaragaike-1 (Tak-1) and all Marchantia

543

mutants and transgenics were cultured on half strength Gamborg's B5 medium (B5 medium,

544

[81]) pH 5.7 supplemented with 1% agar. The Marchantia *mark/praf^{ko}* mutant was previously

545

published as *Mppraf^{ko}* [59].

546

Klebsormidium nitens (NIES-2285) and *Physcomitrium patens* (Gransden strain) was

547

cultured on BCD medium [82] supplemented with 1 % agar under the same condition as M.

548

polymorpha. *Penium margaritaceum* was cultured in liquid Woods Hole medium [83] at pH 7.2

549

under gentle agitation (60RPM) at 20 °C with a 16 h light / 8 dark cycle, 30 – 50 μmol

550

photons m^{-2} s^{-1} light in 50 ml Erlenmeyer flasks.

551

552

Phosphoproteomics

553

Treatment for phosphoproteomics was carried out as described in (Roosjen, Kuhn et al.,

554

accompanying manuscript) with the following adjustments: *Klebsormidium nitens*,

555

Physcomitrium patens and *Marchantia polymorpha* were grown for 10 days on plates as

556

described above, then treated with 100 nM IAA or DMSO in the respective growth medium

557

for 2 minutes, harvested and frozen in liquid nitrogen. *Penium margaritaceum* was grown for

558

15 days as described above. Cells were collected by centrifugation at 1620 g for 2 min and

559

washed 3 times with 10 ml of WHM to remove any residual extracellular polysaccharides

560

from the cell surface. The pellet was resuspended in 10 ml of media and cells were treated

561

with 100 nM IAA or DMSO for 2 min, harvested by centrifugation at 1620 g for 2 min and

562

frozen in liquid nitrogen. Sample preparation and data analysis was carried out as described in

563

(Roosjen, Kuhn et al., accompanying manuscript) with the following adjustments: for

564

Marchantia polymorpha the UP000244005 proteome was used, for *Physcomitrium patens* the

565

UP000006727 proteome was used, for *Klebsormidium nitens* the UP000054558 proteome was

566

used and for *Penium margaritaceum* the proteome from a whole genome assembly was used

567

568 [48]. The mass spectrometry proteomics data, protein lists and intensity values of all samples

569 have been deposited to the ProteomeXchange Consortium via the PRIDE [84] partner repository

570 with the dataset identifier XXX. All phosphoproteomics data has been compiled in the

571 AuxPhos web-app (https://weijerslab.shinyapps.io/AuxPhos; Roosjen, Kuhn et al.,

572 accompanying manuscript).

573

574 **Orthogroup construction**

575 Identification of orthogroups i.e., common orthologous sequences between multiple species

576 were estimated using Orthofinder [85]. Proteomes used for this analysis include: *Arabidopsis*

577 *thaliana* (Araport11), *Marchantia polymorpha* (v6.1), *Physcomitrium patens* (v3.3),

578 *Klebsormidium nitens* (v1.1) and *Penium margaritaceum* (v1).

579

580 **Cytoplasmic streaming**

581 Cytoplasmic streaming was recorded using a Leica SP5 or SP8 confocal microscope equipped

582 with HyD detectors using Apo λ 63×/1.10 water immersion objective plus 6x digital zoom in

583 an 256x256 pixel format. Cytoplasmic streaming was recorded and analyzed for Arabidopsis

584 epidermal cells of the root elongation zone and Marchantia rhizoid cells using the following

585 method: Seven day old Arabidopsis plate-grown seedlings were taken into the microscopy

586 room and mitochondria were stained by transferring the seedling into a petri dish with liquid

587 ½ MS medium containing 1 µM Rhodamine 123 for 5 minutes. Subsequently, seedlings were

588 washed with liquid ½ MS without Rhodamine 123. Seedlings were then transferred to

589 microcopy slides in a drop of liquid ½ MS containing 100 nM IAA or DMSO, covered by a

590 coverslip and left on the microscope stage to adapt to the environment for 30 minutes.

591 Cytoplasmic streaming was recorded in at least 5 epidermal cells of the root elongation zone

592 per root at a frame rate of 5.3 frames per second for 30 seconds (159 frames).

593 Prior to the experiment, Marchantia thallus was grown from gemmae for two days in

594 liquid B5 medium in a petridish. After two days of cultivation Rhodamine 123 was added to a

595 final concentration of 1 µM and Triton-X-100 was added to a final concentration of 0.01%.

596 Marchantia samples were stained for 30 minutes and then washed three time with liquid B5

597 medium containing 0.01% Triton-X-100 without Rhodamine 123. Samples were then

598 transferred to microscopy slides and cytoplasmic streaming in rhizoid cells was recorded as

599 described for Arabidopsis.

600

601 **Data analysis for cytoplasmic streaming**

602 Data analysis was performed in MatLab (version: 2021b). First, static background signal was
603 removed from the raw fluorescence images using a moving window median filter (averaging
604 window = 25 frames) and motile objects smoothed with a 2-pixel Gaussian blur filter. Moving
605 objects were tracked using an established particle tracking algorithm [86], keeping only those
606 trajectories whose length exceeds 3 seconds. For each cell, from the individual trajectories of
607 the remaining moving objects, typically between 30 to 60 per time series, an ensemble-
608 averaged mean-squared displacement was computed:

609

$$\Delta r^2(\tau) = <|r(t+\tau) - r(t)|^2>$$

610

611 Per cell, these mean-squared displacements were fitted to the anomalous diffusion model
612 (ADM) [87,88], a generalization of Einstein's diffusion model to describe complex non-Fickian
613 motion of organelles in the visco-elastic liquid of the cellular cytosol, which is composed of
614 an unknown mixture of passive (Brownian) and active (streaming) transport in a crowded and
615 heterogeneous medium:

616

$$\Delta r^2(\tau) = K\tau^\alpha$$

617

618 where τ is the correlation time. In the ADM, the generalized diffusion power law exponent α
619 provides information on the average nature of the transport processes: $\alpha < 1$ is indicative of
620 sub-diffusive motion, characteristic of Brownian motion in a visco-elastic liquid, $\alpha = 1$
621 indicates pure Brownian motion in a viscous liquid and $\alpha > 1$, known as super-diffusion,
622 indicates transport with an active, e.g., motor-protein driven, component. Intermediate values
623 of the power law exponent α provide insight into the relative balance of these different
624 processes on the organellar motion. The transport rate constant K (in units mm/s^a) informs
625 about the average transport rate: the larger the value of K the faster the organellar transport in
626 the cells. Our analysis yields one average value for α and K per cell; the significance of the
627 differences between control and treatment was assessed with a two-sided Wilcoxon signed
628 rank test.

629

Membrane potential measurement using DISBAC$_2$(3)
631 Membrane potential was measured using the DISBAC$_2$(3) probe as previously described for
632 Arabidopsis[17]. DISBAC2(3) (2 µM) was added to buffered ½ MS liquid medium with 1%

633 (w/v) sucrose containing either 0 or 100 nM IAA. Five-day-old Arabidopsis seedlings were
634 transferred to a sealable single-layer PDMS silicone chip[17]. The PDMS silicone chip
635 containing the seedlings was then placed on a vertical spinning disk microscope for a 20-min
636 recovery. During the recovery process, the seedlings were treated with control medium at a
637 flow rate of 3 µl/min. Seedlings were imaged every 30 seconds with a x20/0.8 objective.
638 DISBAC2(3) was excited with a 515-nm laser, and the emission was filtered with a 535/30-
639 nm bandpass filter. DISBAC2(3) fluorescence was measured at the border between epidermis
640 and cortical cells of the transition zone by selecting 5-6 or 3-4 cells for Col-0 and
641 *Atmark/raf^{null},* respectively.

642 Membrane potential of Marchantia and Klebsormidium was measured using the same
643 probe with the following modifications to the protocol: Marchantia gemmae were removed
644 from gemmae cups and placed liquid B5 with 0.01%Triton-X-100 supplemented with 15 µM
645 $DISBAC_2(3)$, vacuum infiltrated for 5 minutes and transferred to a cover slip followed by
646 incubation for 30 minutes before imaging. Imaging was performed on an inverted Leica SP8
647 confocal microscope using the same setting as for Arabidopsis. Klebsormidium was grown for
648 10 days as described above. A small amount of Klebsormidium was then scraped off the plate
649 and dissolved in liquid BCD medium supplemented with 15 µM $DISBAC_2(3)$ followed by
650 incubation for 30 minutes before imaging.

651

652 **Root surface pH profile**
653 Root surface pH was measured using the ratiometric Fluorescein-5-(and-6)-Sulfonic Acid,
654 Trisodium Salt (FS) (Invitrogen™ F1130)[89]. Five-day-old Arabidopsis seedlings were
655 transferred to unbuffered ½ MS medium containing 50 µM FS dye and either 0 or 100 nM
656 IAA. Seedlings were allowed to recover on a vertical spinning disk microscope for 20 minutes
657 after transfer to the microscope chamber. Imaging was performed using a vertical stage Zeiss
658 Axio Observer 7 microscope coupled to a Yokogawa CSU-W1-T2 spinning disk unit with 50
659 µm pinholes, equipped with a VS-HOM1000 excitation light homogenizer (Visitron
660 Systems). Images were acquired using VisiView software (Visitron Systems, v.4.4.0.14). We
661 used a Zeiss Plan-Apochromat ×10/0.45 objective. FS was excited by 405 and 488 nm laser.
662 The 488/405 nm fluorescence emission ratio along the root was calculated using the ATR
663 software[89].

664

665 **Phenotyping**

666   Arabidopsis ***plant height*** was determined from respectively 48 individual wild type and
667   *mark/raf^{null}* senescing plants, seven weeks after germination. To compare the ***leaf area*** of
668   fully elongated leaf 6 to leaf 9 of Arabidopsis wild type, *mark/raf^{null}* and *mark/raf^{weak}*, 16
669   plants per genotype were collected, flattened on paper and photographed using a Canon EOS
670   250D with EFS 18-135mm Macro Lens. Leaf area was measured in ImageJ (Version 1.52)
671   using the Polygon selection tool.

672   ***Rosette area*** was determined from respectively 90 individual wild type and *mark/raf^{null}* plants
673   plants 28 days after germination. Plants were photographed individually using a Canon EOS
674   250D camera with EFS 18-135mm Macro Lens. Rosette area was then measured in ImageJ
675   (Version 1.52) using the Polygon selection tool. To compare the ***germination efficiency***
676   between *mark/raf^{null}* mutants and wild type, seeds for each genotype were surface sterilized,
677   stratified in a 0.1% agarose solution for two days at 4 °C and paced on half strength MS plates
678   (0.8% Agar). Plates were grown vertically for 9 days and germinated seeds were scored at day
679   1, 2, 3, 4, 7 and 9. Germination percentages were calculated for each day. The experiment was
680   repeated three times individually and data were combined for analysis.

681   Seedlings of Arabidopsis wild type, *mark/raf^{null}* and *mark/raf^{weak}* were germinated on half
682   strength MS and vertically grown for 5 days. After five days, ten seedlings with representative
683   root length for each genotype were transferred to new square petri dishes either containing 1
684   nM IAA, 100 nM IAA or a mock treatment representing an equal amount of solvent (DMSO).
685   ***Root length*** was captured by photographing the plates immediately after transferring the
686   seedlings, after 24 hour, after 48 hours and after 120 hours, using a Canon EOS 250D camera
687   with EFS 18-135mm Macro Lens. Root length was then measured in ImageJ using the
688   segmented line tool and growth rates calculated.

689   To compare the ***thallus growth*** between Marchantia *mark/praf^{ko}* mutants (n=44) and
690   wild type (n=50), thalli were grown from gemmae on half strength Gamborg B5 medium.
691   Plates were grown for 29 days and projected thallus area was captured by photographing the
692   plates immediately after transferring the gemmae, after 2, 4, 7, 9, 11, 14, 16, 18, 22 and 29
693   days, using a Canon EOS 250D camera with EFS 18-135mm Macro Lens. Thallus area was
694   then measured in ImageJ (Version 1.52) using the Polygon selection tool. For ***auxin***
695   ***sensitivity*** assays, Marchantia *mark/praf^{ko}* mutant (n=10) or wild-type (n=10) gemmae were
696   grown on half strength Gamborg B5 medium supplemented the indicated concentration of
697   IAA and grown for 10 days. At day 10, thallus size was captured by photographing the plates
698   using a Canon EOS 250D with EFS 18-135mm Macro Lens. Thallus area was then measured
699   in ImageJ (Version 1.52) using the Polygon selection tool. ***Gemma cup number*** was

700   determined on *mark/praf^{ko}* mutants (n=14) and wild type (n=14) thalli after 24 days of growth

701   on half strength Gamborg B5 medium.

702

Transcriptomic analysis

704   *Arabidopsis thaliana* wild-type (Col-0) and mutant (*mark/raf^{null}*) seeds were sown on half-

705   strength MS medium covered with nylon mesh and vertically grown for 7 days. Plants were

706   then submerged in liquid half-strength MS medium containing either 1 µM IAA or the

707   equivalent amount of solvent (DMSO). Plates were kept horizontally for about 30 seconds

708   and then kept vertically for 1 hour to incubate. After incubation, root tips were harvested

709   using a scalpel and immediately frozen in liquid nitrogen.

710   *Marchantia polymorpha* wild-type (Tak-1) and mutant (*mark/praf^{ko}*) gemmae were

711   placed on B5 solid medium covered with nylon mesh (100 mm pore) and grown for 9 days.

712   After growing, plants were submerged in liquid B5 medium and cultured for 1 day. After pre-

713   cultivation, IAA was added to a final concentration of 1 µM or an equivalent amount of

714   DMSO was added and plants were incubated for 1 hour. Using a scalpel, thalli were harvested

715   from the mesh, blotted on paper towels and immediately frozen in liquid nitrogen.

716   After harvesting, all frozen samples were ground into fine powder using a pre-cooled

717   mortar and pestle. Total RNA form all samples was extracted using a RNeasy Plant Mini Kit

718   (QIAGEN). Total RNA was treated with RNase-free DNase I set (QIAGEN). RNA-seq

719   library construction and RNA sequencing were performed by BGI Tech Solutions (Hong

720   Kong).

721

RNAseq data analysis

723   Up to 20 million paired-end 150 bp reads were collected for each sample. Quality assessment

724   for   raw   reads   was   performed   using   FastQC

725   (www.bioinformatics.babraham.ac.uk/projects/fastqc). For both *Arabidopsis thaliana*

726   (Araport11; [90]) and *Marchantia polymorpha* (v6.1; [91]), reads were mapped onto the

727   respective genomes using HISAT2 (v2.1.0; [92]) with additional parameters "--trim5 10 –dta".

728   Alignment (SAM/BAM) files were sorted and indexed using SAMTOOLS (v1.9;[93]).

729   FeatureCounts (v2.0.0; [94]) was used to count the reads mapped on to each gene, with the

730   parameters "-t 'exon' -g 'gene_id' -Q 30 --primary -p -B -C" for Arabidopsis transcipts and "t

731   'gene' -g 'ID' -Q 30 --primary -p -B -C" for Marchantia transcripts. DEseq2 [95] was used to

732   normalize the raw counts and perform the differential expression analysis with a design

733   matrix including the interaction term (Padj<0.05). Data processing and statistical analysis was

734   performed using R (https://www.r-project.org/). Sequenced raw reads were deposited in NCBI

735   Sequence Read Archive (SRA) under the project accession number PRJNA881051.

736

737   **Generation of transgenics**

738   Primers used in this study can be found in Supplementary Table 1. Arabidopsis MARK

739   reporter lines for MARK1/RAF24 and MARK5/RAF20 under their endogenous promoter

740   were generated by amplifying the genomic fragment including the 3.5 kb region upstream of

741   the start codon using the appropriate primers for each gene. Fragments were cloned into a

742   pGIIK LIC-YFP (pPLV17) vector [96] using the HiFi cloning kit (ThermoFisher).

743   For the Marchantia MARK/PRAF reporter line, a DNA fragment for an Arabidopsis-

744   codon-optimized mCitrine coding sequence (CDS) was synthesized (IDT) and used to amplify

745   a   GGS□2   linker-containing   fragment   by   PCR   with   a   primer   set,

746   pUGW2_Aor_GGS2_mCit_IF_F and pUGW2_Aor_mCit_IF_R, which was then cloned into

747   the Aor51HI site in pUGW2 35S [97] using the In-Fusion cloning kit (TaKaRa Bio). The 2.5-kb

748   HindIII-SacI fragment in the resulting plasmid, including the Gateway cassette followed by

749   the GGS□2 linker-attached mCitrine CDS, was ligated with the HindIII- and SacI-digested

750   pMpGWBx00 [97] to generate pMpGWBx47. The MpMARK/PRAF genomic sequence

751   covering its promoter and CDS (without stop codon) in pENTR/D-TOPO_MpMARK/PRAF

752   [59]   was   transferred   to   pMpGWB347   to   generate   pMpGWB347-MpMARK/PRAF.

753   Agrobacterium GV2260 containing pMpGWB347-MpMARK/PRAF was used to transform

754   Mpmark/praf[ko] plants (Koide et al. 2020) by the thallus transformation method [98].

755

756   **Imaging of transgenic lines plants for MARK-localization analysis:**

757   Marchantia gemmae expressing MARK/PRAF-mCitrine under endogenous promoter and 7

758   day-old Arabidopsis roots expressing MARK1/RAF24-YFP or MARK5/RAF20-YFP under

759   their respective endogenous promoter were imaged using a Leica SP5 or SP8 confocal

760   microscope equipped with an Argon laser (SP5) or a white light laser (SP8). Both, mCitrine

761   and YFP were excited at 514 nm, and emission was collected between 525-575 nm. Images

762   were analyzed using ImageJ (Version 1.52).

763

REFERENCES

1. Friml, J. (2022). Fourteen Stations of Auxin. Cold Spring Harb Perspect Biol *14*, a039859. 10.1101/cshperspect.a039859.

2. Friml, J., Wiśniewska, J., Benková, E., Mendgen, K., and Palme, K. (2002). Lateral relocation of auxin efflux regulator PIN3 mediates tropism in Arabidopsis. Nature *415*, 806–809. 10.1038/415806a.

3. Tao, Y., Ferrer, J.-L., Ljung, K., Pojer, F., Hong, F., Long, J.A., Li, L., Moreno, J.E., Bowman, M.E., Ivans, L.J., et al. (2008). Rapid Synthesis of Auxin via a New Tryptophan-Dependent Pathway Is Required for Shade Avoidance in Plants. Cell *133*, 164–176. 10.1016/j.cell.2008.01.049.

4. Went, F.W., and Thimann, K.V. (1937). Phytohormones (MacMillan Company).

5. Went, F.W. (1928). Wuchsstoff und Wachstum. Recueil des travaux botaniques néerlandais *25*, 1–116.

6. Sessions, R.A., and Zambryski, P.C. (1995). Arabidopsis gynoecium structure in the wild and in ettin mutants. Development *121*, 1519–1532. 10.1242/dev.121.5.1519.

7. Nemhauser, J.L., Feldman, L.J., and Zambryski, P.C. (2000). Auxin and ETTIN in Arabidopsis gynoecium morphogenesis. Development *127*, 3877–3888. 10.1242/dev.127.18.3877.

8. Scarpella, E., Marcos, D., Friml, J., and Berleth, T. (2006). Control of leaf vascular patterning by polar auxin transport. Genes Dev *20*, 1015–1027. 10.1101/gad.1402406.

9. de Rybel, B., Adibi, M., Breda, A.S., Wendrich, J.R., Smit, M.E., Novák, O., Yamaguchi, N., Yoshida, S., van Isterdael, G., Palovaara, J., et al. (2014). Integration of growth and patterning during vascular tissue formation in *Arabidopsis*. Science (1979) *345*. 10.1126/science.1255215.

10. Morffy, N., and Strader, L.C. (2020). Old Town Roads: routes of auxin biosynthesis across kingdoms. Curr Opin Plant Biol *55*, 21–27. 10.1016/j.pbi.2020.02.002.

11. Mutte, S.K., Kato, H., Rothfels, C., Melkonian, M., Wong, G.K.-S., and Weijers, D. (2018). Origin and evolution of the nuclear auxin response system. Elife *7*. 10.7554/eLife.33399.

12. JIN, Q., SCHERP, P., HEIMANN, K., and HASENSTEIN, K. (2008). Auxin and cytoskeletal organization in algae. Cell Biol Int *32*, 542–545. 10.1016/j.cellbi.2007.11.005.

13. Park, W.-K., Yoo, G., Moon, M., Kim, C.W., Choi, Y.-E., and Yang, J.-W. (2013). Phytohormone Supplementation Significantly Increases Growth of Chlamydomonas reinhardtii Cultivated for Biodiesel Production. Appl Biochem Biotechnol *171*, 1128–1142. 10.1007/s12010-013-0386-9.

14. Vance, B.D. (1987). Phytohormone effects on cell division inChlorella pyrenoidosa chick (TX-7-11-05) (chlorellaceae). J Plant Growth Regul *5*, 169–173. 10.1007/BF02087185.

15. Etherton, B. (1970). Effect of Indole-3-acetic Acid on Membrane Potentials of Oat Coleoptile Cells. Plant Physiol *45*, 527–528. 10.1104/pp.45.4.527.

16. Bates, G.W., and Goldsmith, M.H.M. (1983). Rapid response of the plasma-membrane potential in oat coleoptiles to auxin and other weak acids. Planta *159*, 231–237. 10.1007/BF00397530.

808   17.   Serre, N.B.C., Kralík, D., Yun, P., Slouka, Z., Shabala, S., and Fendrych, M. (2021). AFB1
809   controls rapid auxin signalling through membrane depolarization in Arabidopsis
810   thaliana root. Nat Plants *7*, 1229–1238. 10.1038/s41477-021-00969-z.
811   18.   Friml, J., Gallei, M., Gelová, Z., Johnson, A., Mazur, E., Monzer, A., Rodriguez, L.,
812   Roosjen, M., Verstraeten, I., Živanović, B.D., et al. (2022). ABP1–TMK auxin perception
813   for global phosphorylation and auxin canalization. Nature *609*, 575–581.
814   10.1038/s41586-022-05187-x.
815   19.   Ayling, S., and Clarkson, D. (1996). The Cytoplasmic Streaming Response of Tomato
816   Root Hairs to Auxin; the Role of Calcium. Functional Plant Biology *23*, 699.
817   10.1071/PP9960699.
818   20.   Monshausen, G.B., Miller, N.D., Murphy, A.S., and Gilroy, S. (2011). Dynamics of auxin-
819   dependent Ca2+ and pH signaling in root growth revealed by integrating high-
820   resolution imaging with automated computer vision-based analysis. The Plant Journal
821   *65*, 309–318. 10.1111/j.1365-313X.2010.04423.x.
822   21.   Barbez, E., Dünser, K., Gaidora, A., Lendl, T., and Busch, W. (2017). Auxin steers root
823   cell expansion via apoplastic pH regulation in *Arabidopsis thaliana*. Proceedings of the
824   National Academy of Sciences *114*. 10.1073/pnas.1613499114.
825   22.   Shih, H.-W., DePew, C.L., Miller, N.D., and Monshausen, G.B. (2015). The Cyclic
826   Nucleotide-Gated Channel CNGC14 Regulates Root Gravitropism in Arabidopsis
827   thaliana. Current Biology *25*, 3119–3125. 10.1016/j.cub.2015.10.025.
828   23.   Li, L., Verstraeten, I., Roosjen, M., Takahashi, K., Rodriguez, L., Merrin, J., Chen, J.,
829   Shabala, L., Smet, W., Ren, H., et al. (2021). Cell surface and intracellular auxin
830   signalling for H+ fluxes in root growth. Nature *599*, 273–277. 10.1038/s41586-021-
831   04037-6.
832   24.   Senn, A.P., and Goldsmith, M.H.M. (1988). Regulation of Electrogenic Proton Pumping
833   by Auxin and Fusicoccin as Related to the Growth of *Avena* Coleoptiles. Plant Physiol
834   *88*, 131–138. 10.1104/pp.88.1.131.
835   25.   Arieti, R.S., and Staiger, C.J. (2020). Auxin-induced actin cytoskeleton rearrangements
836   require AUX1. New Phytologist *226*, 441–459. 10.1111/nph.16382.
837   26.   Narasimhan, M., Gallei, M., Tan, S., Johnson, A., Verstraeten, I., Li, L., Rodriguez, L.,
838   Han, H., Himschoot, E., Wang, R., et al. (2021). Systematic analysis of specific and
839   nonspecific auxin effects on endocytosis and trafficking. Plant Physiol *186*, 1122–1142.
840   10.1093/plphys/kiab134.
841   27.   Heisler, M.G., Ohno, C., Das, P., Sieber, P., Reddy, G. v., Long, J.A., and Meyerowitz,
842   E.M. (2005). Patterns of Auxin Transport and Gene Expression during Primordium
843   Development Revealed by Live Imaging of the Arabidopsis Inflorescence Meristem.
844   Current Biology *15*, 1899–1911. 10.1016/j.cub.2005.09.052.
845   28.   Dubrovsky, J.G., Sauer, M., Napsucialy-Mendivil, S., Ivanchenko, M.G., Friml, J.,
846   Shishkova, S., Celenza, J., and Benková, E. (2008). Auxin acts as a local morphogenetic
847   trigger to specify lateral root founder cells. Proceedings of the National Academy of
848   Sciences *105*, 8790–8794. 10.1073/pnas.0712307105.
849   29.   Reinhardt, D., Pesce, E.-R., Stieger, P., Mandel, T., Baltensperger, K., Bennett, M.,
850   Traas, J., Friml, J., and Kuhlemeier, C. (2003). Regulation of phyllotaxis by polar auxin
851   transport. Nature *426*, 255–260. 10.1038/nature02081.
852   30.   Thimann, K. v. (1938). HORMONES AND THE ANALYSIS OF GROWTH. Plant Physiol *13*,
853   437–449. 10.1104/pp.13.3.437.

854   31.   Hertel, R., Thomson, K.-St., and Russo, V.E.A. (1972). In-vitro auxin binding to
855   particulate cell fractions from corn coleoptiles. Planta 107, 325–340.
856   10.1007/BF00386394.
857   32.   Kepinski, S., and Leyser, O. (2005). The Arabidopsis F-box protein TIR1 is an auxin
858   receptor. Nature 435, 446–451. 10.1038/nature03542.
859   33.   Dharmasiri, N., Dharmasiri, S., and Estelle, M. (2005). The F-box protein TIR1 is an
860   auxin receptor. Nature 435, 441–445. 10.1038/nature03543.
861   34.   Tan, X., Calderon-Villalobos, L.I.A., Sharon, M., Zheng, C., Robinson, C. v., Estelle, M.,
862   and Zheng, N. (2007). Mechanism of auxin perception by the TIR1 ubiquitin ligase.
863   Nature 446, 640–645. 10.1038/nature05731.
864   35.   Gray, W.M., Kepinski, S., Rouse, D., Leyser, O., and Estelle, M. (2001). Auxin regulates
865   SCFTIR1-dependent degradation of AUX/IAA proteins. Nature 414, 271–276.
866   10.1038/35104500.
867   36.   Kim, J., Harter, K., and Theologis, A. (1997). Protein–protein interactions among the
868   Aux/IAA proteins. Proceedings of the National Academy of Sciences 94, 11786–
869   11791. 10.1073/pnas.94.22.11786.
870   37.   Weijers, D., and Wagner, D. (2016). Transcriptional Responses to the Auxin Hormone.
871   Annu Rev Plant Biol 67, 539–574. 10.1146/annurev-arplant-043015-112122.
872   38.   Prigge, M.J., Platre, M., Kadakia, N., Zhang, Y., Greenham, K., Szutu, W., Pandey, B.K.,
873   Bhosale, R.A., Bennett, M.J., Busch, W., et al. (2020). Genetic analysis of the
874   Arabidopsis TIR1/AFB auxin receptors reveals both overlapping and specialized
875   functions. Elife 9. 10.7554/eLife.54740.
876   39.   Hamann, T., Benkova, E., Bäurle, I., Kientz, M., and Jürgens, G. (2002). The Arabidopsis
877   BODENLOS gene encodes an auxin response protein inhibiting MONOPTEROS-
878   mediated embryo patterning. Genes Dev 16, 1610–1615. 10.1101/gad.229402.
879   40.   Hardtke, C.S., and Berleth, T. (1998). The Arabidopsis gene MONOPTEROS encodes a
880   transcription factor mediating embryo axis formation and vascular development.
881   EMBO J 17, 1405–1411. https://doi.org/10.1093/emboj/17.5.1405.
882   41.   Kato, H., Mutte, S.K., Suzuki, H., Crespo, I., Das, S., Radoeva, T., Fontana, M.,
883   Yoshitake, Y., Hainiwa, E., van den Berg, W., et al. (2020). Design principles of a
884   minimal auxin response system. Nat Plants 6, 473–482. 10.1038/s41477-020-0662-y.
885   42.   Abel, S., and Theologis, A. (1996). Early Genes and Auxin Action. Plant Physiol 111, 9–
886   17. 10.1104/pp.111.1.9.
887   43.   McClure, B.A., Hagen, G., Brown, C.S., Gee, M.A., and Guilfoyle, T.J. (1989).
888   Transcription, organization, and sequence of an auxin-regulated gene cluster in
889   soybean. Plant Cell 1, 229–239. 10.1105/tpc.1.2.229.
890   44.   Fendrych, M., Akhmanova, M., Merrin, J., Glanc, M., Hagihara, S., Takahashi, K.,
891   Uchida, N., Torii, K.U., and Friml, J. (2018). Rapid and reversible root growth inhibition
892   by TIR1 auxin signalling. Nat Plants 4, 453–459. 10.1038/s41477-018-0190-1.
893   45.   Dindas, J., Scherzer, S., Roelfsema, M.R.G., von Meyer, K., Müller, H.M., Al-Rasheid,
894   K.A.S., Palme, K., Dietrich, P., Becker, D., Bennett, M.J., et al. (2018). AUX1-mediated
895   root hair auxin influx governs SCFTIR1/AFB-type Ca2+ signaling. Nat Commun 9, 1174.
896   10.1038/s41467-018-03582-5.
897   46.   Yoon, H.S., Hackett, J.D., Ciniglia, C., Pinto, G., and Bhattacharya, D. (2004). A
898   Molecular Timeline for the Origin of Photosynthetic Eukaryotes. Mol Biol Evol 21,
899   809–818. 10.1093/molbev/msh075.

900   47.   Leebens-Mack, J.H., Barker, M.S., Carpenter, E.J., Deyholos, M.K., Gitzendanner, M.A.,
901   Graham, S.W., Grosse, I., Li, Z., Melkonian, M., Mirarab, S., et al. (2019). One thousand
902   plant transcriptomes and the phylogenomics of green plants. Nature *574*, 679–685.
903   10.1038/s41586-019-1693-2.
904   48.   Jiao, C., Sørensen, I., Sun, X., Sun, H., Behar, H., Alseekh, S., Philippe, G., Palacio Lopez,
905   K., Sun, L., Reed, R., et al. (2020). The Penium margaritaceum Genome: Hallmarks of
906   the Origins of Land Plants. Cell *181*, 1097-1111.e12. 10.1016/j.cell.2020.04.019.
907   49.   Ren, H., Park, M.Y., Spartz, A.K., Wong, J.H., and Gray, W.M. (2018). A subset of
908   plasma membrane-localized PP2C.D phosphatases negatively regulate SAUR-mediated
909   cell expansion in Arabidopsis. PLoS Genet *14*, e1007455.
910   10.1371/journal.pgen.1007455.
911   50.   Takahashi, K., Hayashi, K., and Kinoshita, T. (2012). Auxin Activates the Plasma
912   Membrane H+-ATPase by Phosphorylation during Hypocotyl Elongation in
913   Arabidopsis . Plant Physiol *159*, 632–641. 10.1104/pp.112.196428.
914   51.   Renier, M., Tamanini, A., Nicolis, E., Rolfini, R., Imler, J.-L., Pavirani, A., and Cabrini, G.
915   (1995). Use of a Membrane Potential-Sensitive Probe to Assess Biological Expression
916   of the Cystic Fibrosis Transmembrane Conductance Regulator. Hum Gene Ther *6*,
917   1275–1283. 10.1089/hum.1995.6.10-1275.
918   52.   Tominaga, M., and Ito, K. (2015). The molecular mechanism and physiological role of
919   cytoplasmic streaming. Curr Opin Plant Biol *27*, 104–110. 10.1016/j.pbi.2015.06.017.
920   53.   Huibin Han, Inge Verstraeten, Mark Roosjen, Ewa Mazur, Nikola Rýdza, Jakub Hajný,
921   Krisztina Ötvös, Dolf Weijers, and Jiří Friml (2021). Rapid auxin-mediated
922   phosphorylation of Myosin regulates trafficking and polarity in Arabidopsis. bioRxiv.
923   54.   Songyang, Z., Lu, K.P., Kwon, Y.T., Tsai, L.H., Filhol, O., Cochet, C., Brickey, D.A.,
924   Soderling, T.R., Bartleson, C., Graves, D.J., et al. (1996). A structural basis for substrate
925   specificities of protein Ser/Thr kinases: primary sequence preference of casein kinases
926   I and II, NIMA, phosphorylase kinase, calmodulin-dependent kinase II, CDK5, and Erk1.
927   Mol Cell Biol *16*, 6486–6493. 10.1128/MCB.16.11.6486.
928   55.   Lewis, T.S., Shapiro, P.S., and Ahn, N.G. (1998). Signal Transduction through MAP
929   Kinase Cascades. In, pp. 49–139. 10.1016/S0065-230X(08)60765-4.
930   56.   (Kazuya Ichimura et al.), M.G., Ichimura, K., Shinozaki, K., Tena, G., Sheen, J., Henry, Y.,
931   Champion, A., Kreis, M., Zhang, S., Hirt, H., et al. (2002). Mitogen-activated protein
932   kinase cascades in plants: a new nomenclature. Trends Plant Sci *7*, 301–308.
933   10.1016/S1360-1385(02)02302-6.
934   57.   Shahzad, Z., Canut, M., Tournaire-Roux, C., Martinière, A., Boursiac, Y., Loudet, O., and
935   Maurel, C. (2016). A Potassium-Dependent Oxygen Sensing Pathway Regulates Plant
936   Root Hydraulics. Cell *167*, 87-98.e14. 10.1016/j.cell.2016.08.068.
937   58.   Lin, Z., Li, Y., Zhang, Z., Liu, X., Hsu, C.-C., Du, Y., Sang, T., Zhu, C., Wang, Y., Satheesh,
938   V., et al. (2020). A RAF-SnRK2 kinase cascade mediates early osmotic stress signaling
939   in higher plants. Nat Commun *11*, 613. 10.1038/s41467-020-14477-9.
940   59.   Koide, E., Suetsugu, N., Iwano, M., Gotoh, E., Nomura, Y., Stolze, S.C., Nakagami, H.,
941   Kohchi, T., and Nishihama, R. (2020). Regulation of Photosynthetic Carbohydrate
942   Metabolism by a Raf-Like Kinase in the Liverwort Marchantia polymorpha. Plant Cell
943   Physiol *61*, 631–643. 10.1093/pcp/pcz232.
944   60.   Bowman, J.L., Kohchi, T., Yamato, K.T., Jenkins, J., Shu, S., Ishizaki, K., Yamaoka, S.,
945   Nishihama, R., Nakamura, Y., Berger, F., et al. (2017). Insights into Land Plant

946   Evolution Garnered from the Marchantia polymorpha Genome. Cell *171*, 287-304.e15.
947   https://doi.org/10.1016/j.cell.2017.09.030.

948 61. Benková, E., Michniewicz, M., Sauer, M., Teichmann, T., Seifertová, D., Jürgens, G.,
949   and Friml, J. (2003). Local, Efflux-Dependent Auxin Gradients as a Common Module
950   for Plant Organ Formation. Cell *115*, 591–602. 10.1016/S0092-8674(03)00924-3.

951 62. Flores-Sandoval, E., Eklund, D.M., and Bowman, J.L. (2015). A Simple Auxin
952   Transcriptional Response System Regulates Multiple Morphogenetic Processes in the
953   Liverwort Marchantia polymorpha. PLoS Genet *11*, e1005207.
954   10.1371/journal.pgen.1005207.

955 63. Mutte, S.K., and Weijers, D. (2020). Deep Evolutionary History of the Phox and Bem1
956   (PB1) Domain Across Eukaryotes. Sci Rep *10*, 3797. 10.1038/s41598-020-60733-9.

957 64. Bienz, M. (2014). Signalosome assembly by domains undergoing dynamic head-to-tail
958   polymerization. Trends Biochem Sci *39*, 487–495. 10.1016/j.tibs.2014.08.006.

959 65. Moscat, J., Diaz-Meco, M.T., Albert, A., and Campuzano, S. (2006). Cell Signaling and
960   Function Organized by PB1 Domain Interactions. Mol Cell *23*, 631–640.
961   10.1016/j.molcel.2006.08.002.

962 66. Jakobi, A.J., Huber, S.T., Mortensen, S.A., Schultz, S.W., Palara, A., Kuhm, T., Shrestha,
963   B.K., Lamark, T., Hagen, W.J.H., Wilmanns, M., et al. (2020). Structural basis of
964   p62/SQSTM1 helical filaments and their role in cellular cargo uptake. Nat Commun *11*,
965   440. 10.1038/s41467-020-14343-8.

966 67. Lamark, T., Perander, M., Outzen, H., Kristiansen, K., Øvervatn, A., Michaelsen, E.,
967   Bjørkøy, G., and Johansen, T. (2003). Interaction Codes within the Family of
968   Mammalian Phox and Bem1p Domain-containing Proteins. Journal of Biological
969   Chemistry *278*, 34568–34581. 10.1074/jbc.M303221200.

970 68. Nakamura, K., Uhlik, M.T., Johnson, N.L., Hahn, K.M., and Johnson, G.L. (2006). PB1
971   Domain-Dependent Signaling Complex Is Required for Extracellular Signal-Regulated
972   Kinase 5 Activation. Mol Cell Biol *26*, 2065–2079. 10.1128/MCB.26.6.2065-2079.2006.

973 69. Blagoev, B., Ong, S.-E., Kratchmarova, I., and Mann, M. (2004). Temporal analysis of
974   phosphotyrosine-dependent signaling networks by quantitative proteomics. Nat
975   Biotechnol *22*, 1139–1145. 10.1038/nbt1005.

976 70. Winston, B.W., Lange-Carter, C.A., Gardner, A.M., Johnson, G.L., and Riches, D.W.
977   (1995). Tumor necrosis factor alpha rapidly activates the mitogen-activated protein
978   kinase (MAPK) cascade in a MAPK kinase kinase-dependent, c-Raf-1-independent
979   fashion in mouse macrophages. Proceedings of the National Academy of Sciences *92*,
980   1614–1618. 10.1073/pnas.92.5.1614.

981 71. Tominaga, M., Kimura, A., Yokota, E., Haraguchi, T., Shimmen, T., Yamamoto, K.,
982   Nakano, A., and Ito, K. (2013). Cytoplasmic Streaming Velocity as a Plant Size
983   Determinant. Dev Cell *27*, 345–352. 10.1016/j.devcel.2013.10.005.

984 72. Du, M., Spalding, E.P., and Gray, W.M. (2020). Rapid Auxin-Mediated Cell Expansion.
985   Annu Rev Plant Biol *71*, 379–402. 10.1146/annurev-arplant-073019-025907.

986 73. Folta, K.M., and Spalding, E.P. (2001). Unexpected roles for cryptochrome 2 and
987   phototropin revealed by high-resolution analysis of blue light-mediated hypocotyl
988   growth inhibition. The Plant Journal *26*, 471–478. 10.1046/j.1365-313x.2001.01038.x.

989 74. Kato, H., Ishizaki, K., Kouno, M., Shirakawa, M., Bowman, J.L., Nishihama, R., and
990   Kohchi, T. (2015). Auxin-Mediated Transcriptional System with a Minimal Set of
991   Components Is Critical for Morphogenesis through the Life Cycle in Marchantia
992   polymorpha. PLoS Genet *11*, e1005084. 10.1371/journal.pgen.1005084.

75. Yu, Y., Tang, W., Lin, W., Zhou, X., Li, W., Li, Y., Chen, R., Cao, W., Perez-Henriquez, P., Huang, R., et al. (2022). ABLs and TMKs are co-receptors for extracellular auxin.

76. Khuri, S., Bakker, F.T., and Dunwell, J.M. (2001). Phylogeny, Function, and Evolution of the Cupins, a Structurally Conserved, Functionally Diverse Superfamily of Proteins. Mol Biol Evol 18, 593–605. 10.1093/oxfordjournals.molbev.a003840.

77. Murashige, T., and Skoog, F. (1962). A revised medium for rapid growth and bio assays with tobacco tissue cultures. Physiol Plant 15, 473–497.

78. Dai, N., Wang, W., Patterson, S.E., and Bleecker, A.B. (2013). The TMK Subfamily of Receptor-Like Kinases in Arabidopsis Display an Essential Role in Growth and a Reduced Sensitivity to Auxin. PLoS One 8, e60990-.

79. Gao, Y., Zhang, Y., Zhang, D., Dai, X., Estelle, M., and Zhao, Y. (2015). Auxin binding protein 1 (ABP1) is not required for either auxin signaling or *Arabidopsis* development. Proceedings of the National Academy of Sciences 112, 2275–2280. 10.1073/pnas.1500365112.

80. Savaldi-Goldstein, S., Baiga, T.J., Pojer, F., Dabi, T., Butterfield, C., Parry, G., Santner, A., Dharmasiri, N., Tao, Y., Estelle, M., et al. (2008). New auxin analogs with growth-promoting effects in intact plants reveal a chemical strategy to improve hormone delivery. Proceedings of the National Academy of Sciences 105, 15190–15195. 10.1073/pnas.0806324105.

81. Gamborg, O.L., Miller, R.A., and Ojima, K. (1968). Nutrient requirements of suspension cultures of soybean root cells. Exp Cell Res 50, 151–158. 10.1016/0014-4827(68)90403-5.

82. Cove, D.J., Perroud, P.-F., Charron, A.J., McDaniel, S.F., Khandelwal, A., and Quatrano, R.S. (2009). Culturing the Moss Physcomitrella patens. Cold Spring Harb Protoc 2009, pdb.prot5136. 10.1101/pdb.prot5136.

83. Domozych, D.S., Sørensen, I., Popper, Z.A., Ochs, J., Andreas, A., Fangel, J.U., Pielach, A., Sacks, C., Brechka, H., Ruisi-Besares, P., et al. (2014). Pectin Metabolism and Assembly in the Cell Wall of the Charophyte Green Alga Penium margaritaceum. Plant Physiol 165, 105–118. 10.1104/pp.114.236257.

84. Perez-Riverol, Y., Bai, J., Bandla, C., García-Seisdedos, D., Hewapathirana, S., Kamatchinathan, S., Kundu, D.J., Prakash, A., Frericks-Zipper, A., Eisenacher, M., et al. (2022). The PRIDE database resources in 2022: a hub for mass spectrometry-based proteomics evidences. Nucleic Acids Res 50, D543–D552. 10.1093/nar/gkab1038.

85. Emms, D.M., and Kelly, S. (2019). OrthoFinder: phylogenetic orthology inference for comparative genomics. Genome Biol 20, 238. 10.1186/s13059-019-1832-y.

86. Gao, Y., and Kilfoil, M.L. (2009). Accurate detection and complete tracking of large populations of features in three dimensions. Opt Express 17, 4685. 10.1364/OE.17.004685.

87. Metzler, R., Jeon, J.-H., Cherstvy, A.G., and Barkai, E. (2014). Anomalous diffusion models and their properties: non-stationarity, non-ergodicity, and ageing at the centenary of single particle tracking. Phys. Chem. Chem. Phys. 16, 24128–24164. 10.1039/C4CP03465A.

88. Regner, B.M., Vučinić, D., Domnisoru, C., Bartol, T.M., Hetzer, M.W., Tartakovsky, D.M., and Sejnowski, T.J. (2013). Anomalous Diffusion of Single Particles in Cytoplasm. Biophys J 104, 1652–1660. 10.1016/j.bpj.2013.01.049.

1038 89. Serre, N.B., Wernerova, D., Vittal, P., Dubey, S.M., Medvecka, E., Jelinkova, A.,
1039   Petrasek, J., Grossmann, G., and Fendrych, M. (2022). The AUX1-AFB1-CNGC14
1040   module establishes longitudinal root surface pH profile. bioRxiv.
1041 90. Cheng, C., Krishnakumar, V., Chan, A.P., Thibaud-Nissen, F., Schobel, S., and Town,
1042   C.D. (2017). Araport11: a complete reannotation of the *Arabidopsis thaliana* reference
1043   genome. The Plant Journal *89*, 789–804. 10.1111/tpj.13415.
1044 91. Montgomery, S.A., Tanizawa, Y., Galik, B., Wang, N., Ito, T., Mochizuki, T., Akimcheva,
1045   S., Bowman, J.L., Cognat, V., Maréchal-Drouard, L., et al. (2020). Chromatin
1046   Organization in Early Land Plants Reveals an Ancestral Association between
1047   H3K27me3, Transposons, and Constitutive Heterochromatin. Current Biology *30*, 573-
1048   588.e7. 10.1016/j.cub.2019.12.015.
1049 92. Kim, D., Langmead, B., and Salzberg, S.L. (2015). HISAT: a fast spliced aligner with low
1050   memory requirements. Nat Methods *12*, 357–360. 10.1038/nmeth.3317.
1051 93. Li, H., Handsaker, B., Wysoker, A., Fennell, T., Ruan, J., Homer, N., Marth, G., Abecasis,
1052   G., and Durbin, R. (2009). The Sequence Alignment/Map format and SAMtools.
1053   Bioinformatics *25*, 2078–2079. 10.1093/bioinformatics/btp352.
1054 94. Liao, Y., Smyth, G.K., and Shi, W. (2014). featureCounts: an efficient general purpose
1055   program for assigning sequence reads to genomic features. Bioinformatics *30*, 923–
1056   930. 10.1093/bioinformatics/btt656.
1057 95. Love, M.I., Huber, W., and Anders, S. (2014). Moderated estimation of fold change
1058   and dispersion for RNA-seq data with DESeq2. Genome Biol *15*, 550. 10.1186/s13059-
1059   014-0550-8.
1060 96. de Rybel, B., van den Berg, W., Lokerse, A.S., Liao, C.-Y., van Mourik, H., Möller, B.,
1061   Llavata-Peris, C.I., and Weijers, D. (2011). A Versatile Set of Ligation-Independent
1062   Cloning Vectors for Functional Studies in Plants   . Plant Physiol *156*, 1292–1299.
1063   10.1104/pp.111.177337.
1064 97. Ishizaki, K., Nishihama, R., Ueda, M., Inoue, K., Ishida, S., Nishimura, Y., Shikanai, T.,
1065   and Kohchi, T. (2015). Development of Gateway Binary Vector Series with Four
1066   Different Selection Markers for the Liverwort Marchantia polymorpha. PLoS One *10*,
1067   e0138876. 10.1371/journal.pone.0138876.
1068 98. KUBOTA, A., ISHIZAKI, K., HOSAKA, M., and KOHCHI, T. (2013). Efficient *Agrobacterium*
1069   -Mediated Transformation of the Liverwort *Marchantia polymorpha* Using
1070   Regenerating Thalli. Biosci Biotechnol Biochem *77*, 167–172. 10.1271/bbb.120700.
1071 99. Woo, E.-J. (2002). Crystal structure of auxin-binding protein 1 in complex with auxin.
1072   EMBO J *21*, 2877–2885. 10.1093/emboj/cdf291.
1073

1074

1075

1076

1077   **FIGURE LEGENDS**

1078

1079   **Figure 1 Comparative phosphoproteomics identifies a rapid and conserved auxin**

1080   **response.** (A) Distribution histograms of significant differential phosphosites (FDR≤0.05)

1081   comparing 2 minutes of 100 nM IAA (Auxin) treatment with mock treatment across 5 species.

1082   Numbers of hyper- or hypo-phosphorylated sites are indicated. (B) Strategy for orthogroup

1083   based on protein sequence across the 5 species used here (top). The lower panel shows the

1084   number proteins residing in shared (black) and unique (grey) orthogroups in each species. (C)

1085   Venn diagram depicting the orthogroups found as differentially phosphorylated upon auxin

1086   treatment in all 5 species. (D) Reduced GO analysis (Revigo) of the 29 shared orthogroups

1087   (marked green in panel C). Circle sizes correspond to gene count within orthogroups. (E)

1088   Heatmap depicting measured significantly differential phosphosites (FDR≤0.05) of two

1089   kinase families, PHOT and RAF-like kinases. (F) Venn diagram depicting the number of

1090   shared GO terms across all species tested, based on closest Arabidopsis homolog of each

1091   differential protein (FDR≤0.05). (G) Reduced GO analysis (Revigo) of the 7 shared

1092   orthogroups (marked green in panel F). (H) Differential phosphorylation of plasma membrane

1093 H^+-ATPases across all species tested.

1094

1095   **Figure 2 Auxin triggers fast cellular and physiological responses across the plant**

1096   **kingdom**

1097   (A) Scheme depicting membrane polarity and depolarization measured using DISBAC2(3)

1098   fluorescence (left) and normalized fluorescence in control (mock) and IAA-treated

1099   Arabidopsis root cells, Marchantia thallus cells and Klebsormidium cells. (B) Scheme

1100   depicting cytoplasmic streaming (left) and diffusion rate K (μm^{α}/s) in control (mock) and

1101   IAA-treated Arabidopsis root cells and Marchantia thallus. Boxplots are shown along

1102   individual measurements, number of observations (n) is indicated, and significance (Student's

1103   t-test) is shown.

1104

1105   **Figure 3. Identification of MARK/RAF-like kinases.**

1106   **(A)** Clustering of phosphomotif enrichment scores (using motifeR) of significantly

1107   differential (FDR≤0.05) phosphosites in all tested species. **(B)** Raw MS1 intensities of RAF-

1108   like kinase orthologues in mock- and IAA-treated samples. Phosphorylated residues are

1109   indicated. Lower: domain topology of B4 RAF-like kinases indicating positions of PB1 and

1110   kinase domains (residue numbers) in Arabidopsis MARK5/Raf24 (At), Marchantia

1111   MARK/PRAF (Mp), Physcomitrium MARK (Pp) and Klebsormidium MARK (Kn). **(C)**

1112   Inferred phylogeny of the B4 RAF-like kinase. Arabidopsis numbering is indicated on the top.

1113   Every node represents an inferred ancestral gene copy at each divergence event. The complete

1114   tree can be found at interactive Tree of Life (iTOL): https://itol.embl.de/shared/dolfweijers.

1115   **(D)** Phenotype of Arabidopsis (left) Col-0 wild-type and *mark/raf* null mutant rosettes and

1116   Marchantia (right) Tak-1 wild-type and *mark/praf* mutants thallus **(E,F)** Length of Col-0

1117   wild-type and *mark/raf* mutant Arabidopsis roots **(E)** and area of Tak-1 wild-type and

1118   *mark/praf* mutant Marchantia thallus **(F)** on increasing concentrations of IAA. Distributions at

1119   each concentration were tested for significant differences using ANOVA.

1120

1121   **Figure 4. MARK mediates auxin posphoresponse across land plant species.**

1122   **(A,B)** PCA plots (left) and expression analysis of individual, auxin-regulated genes (right)

1123   from RNA-seq analysis on (Col-0; Tak-1) wildtype and *mark* mutants in Arabidopsis roots

1124   and Marchantia gemmae treated with 1μM IAA for 1 hour. **(C)** Distribution histograms of

1125   significant differential phosphosites (FDR≤0.05) comparing 2 minutes of 100 nM IAA

1126   (Auxin) treatment with mock treatment in wild-type (dashed lines) and mark mutant (solid

1127   area) Arabidopsis roots (top) and Marchantia gemmae (bottom). Number of phosphosites is

1128   indicated. **(D)** Venn diagrams indicating orthogroup overlap of significantly differential

1129   phosphosites (FDR≤0.05) in *mark* mutants in Arabidopsis and Marchantia compared to

1130   respective wild-types under mock condition. **(E)** Venn diagrams indicating orthogroup

1131   overlap of significantly differential phosphosites (FDR≤0.05) in *mark* mutants and wild-types

1132   in Arabidopsis and Marchantia under IAA-treated condition. **(F).** Gene ontology analysis on

1133   the overlapping and conserved auxin- and MARK-dependent proteins. **(G,H)** Heatmap

1134   showing differential phosphorylation in Arabidopsis **(G)** and Marchantia **(H)** *mark* mutants of

1135   all kinases that are auxin-regulated in wild-type.

1136

1137   **Figure 5. Requirements of MARK activation and activity**

1138   **(A)** Heatmap showing phosphorylation profiles, normalized to the t=0 timepoint, of

1139   Arabidopsis MARK/RAF kinases (data from Roosjen-Kuhn et.al., accompanying

1140   manuscript). Profiles marked with asterisk and red name are phosphosites located in the

1141   activation loop. **(B)** Chord plot depicting overlap between significant (FDR≤0.05)

1142   phosphosites in Arabidopsis mutants challenged with auxin (red) or without (blue). Overlap

1143   shows that the *mark/raf* mutant shares more commonly regulated phosphosites with *tmk1-1*

1144   *and abp1-TD1* mutants than with the *afb1-3* mutant. **(C)** Z-scored MS1 intensities off all

1145   measured phosphosites of Arabidopsis MARK/RAF kinases in wild-type, *afb1-3*, *tmk1-1* and

1146   *abp1-TD1* mutants with or without IAA. **(D)** Principal component analysis of Z-scored MS1

1147   intensities of all 1048 phosphosites that are auxin-regulated in wild-type in control- and

1148   auxin-treated wildtype, *tmk1-1, abp1-TD1 and afb1-3* mutants.

1149

1150   **Figure 6 MARK links rapid phospho-response to fast auxin responses**

1151   (**A**) Fluorescence of Arabidopsis MARK5/RAF20-TurboID-sYFP, driven from its

1152   endogenous promoter, in primary root tips. Right panel shows close-up of epidermal cells. **(B)**

1153   Fluorescence of Marchantia MARK/PRAF-Citrine driven from its endogenous promoter in

1154   gemma. Right panel shows close-up of rhizoid initial cells. **(C)** Analysis of membrane

1155   depolarization on Arabidopsis and Marchantia *mark* mutants in mock and IAA-treated root

1156   (Arabidopsis) and thallus (Marchantia) cells (compare to Figure 2 A for wild types).

1157   Displayed is the normalized DISBAC2(3) fluorescence (IAA/mock). **(D)** Cytoplasmic

1158   streaming in Arabidopsis and Marchantia *mark* mutants in mock and IAA-treated root

1159   (Arabidopsis) and thallus (Marchantia) cells (compare to Figure 2B for wild types). Displayed

1160   is the Diffusion rate K (μm^{α}/s). Boxplots are shown along individual measurements, number

1161   of observations (n) is indicated, and significance (Student's t-test) is shown.

1162

1163   **Supplementary figure 1. Cytoplasmic streaming relies on the actin cytoskeleton** (A,B)

1164   Quantification of the diffusive component (α) of cytoplasmic streaming in wild-type and

1165   *mark/raf* mutant Arabidopsis roots (**A**) and wild-type and Atmark/praf mutant Marchantia

1166   thallus (**B**) with and without auxin treatment. (C,D) Diffusive Exponent (α; C) and Diffusion

1167   Rate (K; D) of cytoplasmic streaming in wild-type Arabidopsis roots treated with mock

1168   medium or Lantrunculin B. Boxplots are shown along individual measurements, number of

1169   observations (n) is indicated, and significance (Student's t-test) is shown.

1170

1171

1172 **Supplementary figure 2 Phenotypic analysis of *mark* mutants in Marchantia and**
1173 **Arabidopsis**

1174 (**A**) Projected thallus area in wild-type and *Mpmark/praf^{ko}* mutant Marchantia thallus,
1175 followed over 29 days. (**B**) Number of gemma cup on wild-type and *Mpmark/praf^{ko}* mutant
1176 Marchantia thallus. (**C**). Root length in wild-type and *mark/raf^{null}* mutant Arabidopsis
1177 seedlings, followed over 9 days. (**D,E**) Rosette area (**D**) and height (**E**) in wild-type and
1178 *mark/raf^{null}* mutant Arabidopsis plants. (**F**) Germination rate of wild-type and *mark/raf^{null}*
1179 mutant Arabidopsis seeds, followed over 9 days. (**G,H**) Examples of images used for
1180 quantification in panel **A** and **C**, respectively.

1181

1182 **Supplementary figure 3: Analysis of *mark* mutant phosphoproteomes.**
1183 (**A**) Overlap of MARK targets in Arabidopsis and Marchantia, based on differential
1184 phosphorylation in *Atmark/raf* and *Mpmark/praf* phosphoproteomes under mock conditions,
1185 compared to wild-types. (**B**) Venn diagram showing overlap between phosphosites
1186 differentially regulated (≤0.05) in mannitol-treated Arabidopsis plants (Lin et.al. 2020),
1187 100nM IAA treated Col-0 and 100nM treated *mark* null mutant. (**C**) Gene identifiers of
1188 Arabidopsis MARK/Raf kinases.

1189

1190 **Supplementary Figure 4: Dynamics of membrane potential in wild-type and *mark/raf***
1191 **mutant Arabidopsis roots**
1192 (**A**) Arabidopsis wildtype (Col-0) and *mark/raf^{null}* mutant root surface pH visualized using the
1193 ratiometric pH-sensitive FS dye treated with mock or 100 nM IAA; scale bar = 50 μm. (**B**)
1194 Quantification of the F488/405 nm fluorescence emission ratio along the root surface of
1195 wildtype (Col-0) and *mark/raf^{null}*. Higher ratio corresponds to alkaline pH. Control and 100
1196 nM IAA-treated roots are shown. The graphs show the averages 12 and 11 roots for wildtype
1197 (Col-0) and *mark/raf^{null}*, respectively for both mock and IAA conditions. Shaded areas
1198 represent standard deviations. (**C**) Dynamics of membrane potential after treatment with 100
1199 nM IAA (arrow) in *Atmark/raf^{null}* (n=10), Col-0 (n=6) and *afb1-3* (n=6) roots. Membrane
1200 potential was visualized by the relative change of the DISBAC2(3) fluorescence over time in
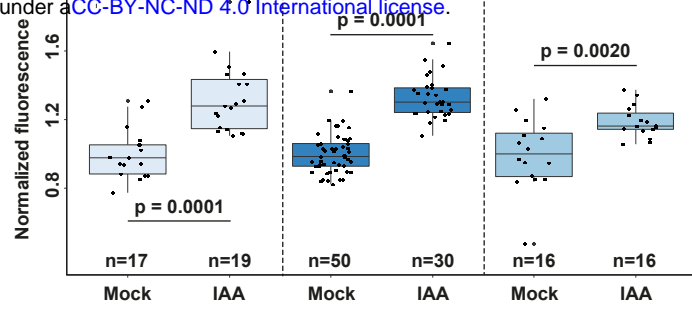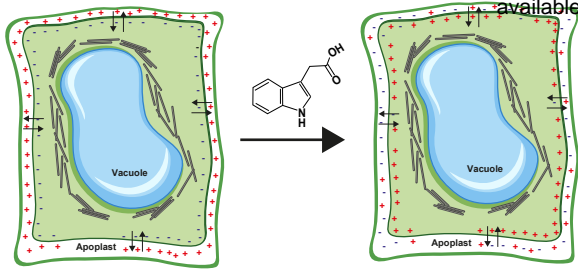1201 a microfluidic chip. Average values are shown, shaded areas represent standard deviations.

1202

1203 **Supplementary figure 6 Phylogenetic analysis of ABP1.**

1204　**(A)** Phylogenetic tree of the ABP1 gene family with green algae and land plant homologs.

1205　Branches that are well-supported (bootstrap >75) are marked with dots. Orthologs from each

1206　phylum are represented with a different color. **(B)** Deep conservation of key amino acids in

1207　the ABP1 auxin binding pocket, as well as the Zinc binding site. Light blue to dark blue color

1208　gradient represents low to high conservation, respectively. Numbering on the top is based on

1209　maize ABP1 protein [99]. The complete tree can be found at interactive Tree of Life (iTOL):

1210　https://itol.embl.de/shared/dolfweijers.

A

Membrane depolarization

B

Cytoplasmic streaming

A

Time (min)

0   0.5   1   2   5   10

MARK5/RAF20 S 867
MARK2/RAF35 S 169
MARK5/RAF20 S 130
* MARK5/RAF20 S 685
* MARK4/RAF18 S 611
MARK3,4,5,7/RAF16,18,20,40 T1125
MARK4,5/RAF18,20 S1003
MARK1/RAF24 S 777
MARK5/RAF20 S 915
MARK4/RAF18 S 811
MARK1/RAF24 S 555
MARK5/RAF20 S 155
MARK4/RAF18 S 311
MARK5/RAF20 S 724
MARK1/RAF24 S 474
MARK5/RAF20 S 655

-2   0   2
Normalized auxin profile

B

Auxin
Mock

abp1-TD1
afb1-1
afb1-3
tmk1-1
abp1-TD1
afb1-3
Col-0
mark/raf null
mark/raf null

C

abp1-TD1 mock
           IAA
tmk1-1   mock
           IAA
afb1-3   mock
           IAA
Col-0   mock
           IAA

MARK4 671/RAF18
MARK1/RAF24 777
MARK5/RAF20 900
MARK4 611/RAF18
MARK5/RAF20 130
MARK4 683/RAF18
MARK2/RAF35 220
MARK7/RAF40 1128
MARK1/RAF24 555
MARK2/RAF35 169
MARK1/RAF24 125
MARK1/RAF24 313
MARK5/RAF20 155
MARK2/RAF35 240
MARK2/RAF35 749
MARK2/RAF35 557
MARK2/RAF35 257
MARK4/RAF18 780
MARK5/RAF20 915
MARK4/RAF18 811
MARK5/RAF20 323
MARK4/RAF18 724
MARK4/RAF18 311
MARK2/RAF35 258

-1.5 -0.5 0.5 1.5
Z-scored MS1 intensities

D

PC2 (25.6%)
PC1 (28.74%)

Genotype
Col-0
abp1-TD1
afb1-3
mark/raf null
tmk1-1

Condition
● IAA
▲ MOCK

A MpMARKL/RAF20-TurboID-sYFP

B MpMARKL/RAF-mCitrine

C

Normalized.fluorescence

| n=10 | n=10 | n=35 | n=20 |

p = 0.0001

p = 0.0001

Mock   IAA   Mock   IAA

D

Diffusion rate K ($\mu m^{\alpha}/s$)

| n=54 | n=54 | n=11 | n=10 |

p= 0.8386

p= 0.1824

Mock   IAA   Mock   IAA